

Hidden Granular Superconductivity Above 500K in off-the-shelf graphite materials

Raphaël Rousset-Zenou,¹ Samar Layek,^{1,*} Miguel Monteverde,²

Frédéric Gay,¹ Didier Dufeu,¹ and Manuel Núñez-Regueiro^{1,†}

¹*Institut Néel, Université Grenoble Alpes and Centre National de la Recherche Scientifique
25 rue des Martyrs - BP 166, 38042, Grenoble cedex 9 France*

²*Laboratoire de Physique des Solides, CNRS-Université Paris-Sud UMR 8502,
91405 Orsay Cedex, France*

(Dated: July 20, 2022)

It has been reported that graphite hosts room temperature superconductivity. Here we provide new results that confirm these claims on different samples of highly oriented pyrolytic graphite (HOPG) and commercial flexible graphite gaskets (FGG). After subtraction of the intrinsic graphite diamagnetism, magnetization measurements show convoluted ferromagnetism and superconducting-like hysteresis loops. The ferromagnetism is deconvoluted by fitting with a sigmoidal function and subtracting it from the data. The obtained superconducting-like hysteresis loops are followed to the highest available temperature, 400K. The extrapolation of the decrease of its moment width with temperature indicates a transition temperature $T_c \sim 550\text{K} \pm 50\text{K}$ for all samples. Electrical resistance measurements confirm the existence at these temperatures of a transition in HOPG samples, albeit without percolation. Besides, the FGG show transitions at temperatures (70K, 270K) near to those reported previously on intercalated-deintercalated graphite, confirming the general character of these superconducting transitions. These results are the first steps in the unveiling of the above room temperature superconductivity of graphite.

Introduction

The quest for superconducting materials started with metals like mercury¹ with superconducting critical temperature $T_c=4.1\text{K}$ more than a century ago. Then alloys from the A-15 compounds, reached a $T_c=22.3\text{K}$ in Nb_3Ge^2 . Followed oxides³, that allowed to reach liquid nitrogen temperatures with YBCO ($T_c=90\text{K}$), the highest value for cuprates being $T_c=166\text{K}$ in fluorinated Hg-1223, under a pressure of 26GPa^4 . Lately, hydrogen derived materials in the extremely high pressures of 200GPa , scratched the room temperature goal^{5,6}.

On the other hand, for more than twenty years there have been recurrent claims for the existence of unidentified microscopic amounts of ferromagnetism and room temperature superconductivity in different types of graphite, i.e. highly oriented pyrolytic graphite (HOPG) and natural single crystals of AB (Bernal) and ABC (rhombohedral)⁸⁻¹⁰. Its origin has been tracked down to granular superconductivity in graphite interfaces¹¹, and its transition temperature is obviously above room temperature.

While, in the last few years, Chern ferromagnetic insulating states¹² and associated superconductivity¹³ have been observed in nano devices made of a few layers of AA graphene twisted at a magic angle. The generated Moiré patterns can be viewed as hyper atoms that yield extremely flat bands^{14,15}. Although the superconducting transition temperatures for these systems are in the range of liquid helium, they stress the need of a deeper inspection of the possible superconducting properties of all type of graphene stacking materials.

Both studies on layered carbon aim at determining the ferromagnetic and superconducting properties of pure graphite, the former being a top-bottom while the latter a bottom-up approach. Whereas the second implies extremely difficult to make but very controlled and defined samples, the first is more like finding a needle in a haystack. For example, if we believe that "magic angles" can explain the claims of superconductivity in bulk graphite, due to the innumerable angles with which graphene planes can be stacked in a macroscopic sample, the amount of regions having the appropriate geometry should be really tiny and difficult to pin down.

Recently, an independent confirmation of room temperature superconductivity in graphite has been reported¹⁶. Superconducting transitions with several high temperature T_c 's, 110K , 245K , 320K , have been observed in KC_8 deintercalated at room temperature¹⁶(IDI samples). The low kinetics of such transformation induces a bulk twisted graphite that scans different twist angles and dopings, yielding a small number of crystallites that have the properties for being superconductors. The superconductivity is granular, although almost percolation has been found for the transition at 245K .

Tracking down with a magnetometer the T_c of a granular superconductivity, due to a few isolated superconducting grains of nanoscopic size in a diamagnetic material such as graphite, is far from evident. The first obvious step is to subtract the large linear intrinsic diamagnetic contribution. Often we are left with a mixed ferromagnetic-superconducting-like hysteresis loop. It must then be deconvoluted fitting a sigmoidal ferromagnetic signal that is then subtracted^{16,17}, yielding the superconducting superconducting-like hysteresis loop. The variation of this cycle with temperature is then measured. The observed cycle shrinking must be followed¹⁶ till its disappearance at T_c . The formula derived from Bean's theory¹⁸ used in applied superconductivity to estimate the critical current J_c is then employed, i.e. the cycle thickness $\Delta M(H,T) \sim J_c(H,T) \sim [1 - (T/T_c)^2]$. Fitting¹⁶ the data to this expression then determines T_c . In the case where T_c is beyond the temperature range of the magnetometer, its uncertainty will be larger the farther away it is.

We have applied this methodology to probe the existence of above room temperature superconductivity on several

samples of commercial, off-the-shelf, forms of graphite. Namely, HOPG and flexible graphite gaskets for industrial applications.

Results

We start describing results on HOPG, where room temperature superconductivity was first reported⁸. We show results for three samples, S1 and S2 issued from the same HOPG ZYA slab, and S3 from a HOPG ZYH (see Table I for a summary of all samples). We show on Fig. 1a a superconducting-like hysteresis loop measured at 50K. We see in the inset of Fig. 1a the strong linear diamagnetic contribution expected for graphite. The first step in analyzing the data is to subtract the linear in field diamagnetic contribution. As shown on Fig. 1, a ferromagnetic cycle becomes then apparent^{8,19}. A clear bulge, though, is present at low fields. If we change the value of the linear diamagnetic correction in $\pm 10\%$ around the optimal value, the bulge is always visible, even when the ferromagnetic sigmoidal cycle is totally deformed. The shape of the shown curve is similar to that obtained from samples having a mixture of superconductivity and ferromagnetism, e.g. Fig. 4 of Ref. 20. In these cases the bulge has been demonstrated to correspond to the presence of superconductivity in the sample. Now, we must extract the superconducting from the ferromagnetic signal. For that we use the known procedure to separate the superconducting-like hysteresis loop from the measurement, as described in Refs. 16 and 17. A sigmoidal function is fitted, corresponding to the ferromagnetic behavior, and then subtracted from the data. The deconvoluted superconducting-like hysteresis loop can be observed on Fig. 1b. The cycle is compatible with a superconducting state.

The cycle, though, does not start at the zero of magnetization, which according to Bean's model¹⁸, implies that a large number of vortices have entered the sample in preceding measurements. As before doing this particular cycle the sample had been annealed by heating it to the maximum available temperature, i.e. 400K, we conclude that the superconducting transition temperature is higher than this value.

The evolution with temperature of the ferromagnetic cycles obtained by subtraction of the measured diamagnetic linear contribution of bulk graphite for S2 is shown on Fig. 1c. The cycles diminish in amplitude, collapsing above 150K. It is clear that the superconducting bulge is still there when ferromagnetism disappears, occupying almost all the thickness of the cycle at 200K.

The saturation moment M_s , defined in Fig. 1, is extracted from each curve and plot as a function of temperature to analyze its evolution (Fig. 1d). It is fitted by the known²¹ phenomenological expression(1) for a ferromagnet below the Curie temperature T_0 , M_0 being the saturation magnetization at 0K.

$$M_s(T, H) = M_0(H)[1 - (T/T_0)^2]^{1/2} \quad (1)$$

The temperature dependence for the three samples is similar but not identical. For sample S1 $T_0=230\text{K}$, S2 $T_0=150\text{K}$, and even if it does not disappear completely for S3 $T_0=350\text{K}$. The values of the saturation magnetization at 0K are: for S1 $M_0=0.0017\text{emu/gr}(3.4 \times 10^{-5} \mu_B \text{ per carbon atom})$, for S2 $M_0=0.009 \text{ emu/gr}(1.8 \times 10^{-5} \mu_B \text{ per carbon atom})$ and S3 $M_0=0.01\text{emu/gr}(2 \times 10^{-5} \mu_B \text{ per carbon atom})$. These values correspond in the average to $\sim 1 \times 10^{-5} \mu_B$ per carbon atom.

The evolution with temperature of the cycles obtained by subtraction of the bulk graphite linear diamagnetism and, only below 150K, of the ferromagnetic sigmoidal evolution is shown for sample S2 on Fig. 2a. It is clear that the amplitude of the cycle decreases with increasing temperature but it is still non-zero at 350K. Assuming Bean's model¹⁸, then $\Delta M(H, T)$, as defined in Fig. 1b, is proportional to $J_c(H, T)$, that follows with temperature the expression

(2). We thus plot on Fig. 2b the $\Delta M(H,T)$ as a function of temperature for samples S1, S2 and S3, and fit them with expression (2). The result yields for three samples an average $T_c \sim 550 \pm 20$ K.

$$J_c(T) = J_{c0}[1 - (T/T_c)^2] \quad (2)$$

With these T_c values as a guide, we measured the electrical resistance at high temperatures on several samples. The results on two pieces of the HOPG ZYA slab, S4 and S5, are shown on Fig. 2c and d, respectively. A clear kink in the linear variation of the resistivity of S4 and a small jump for S5 is observed. Calculating the derivative allows a better precision in the determination of its position. Its shape point to an onset $T_c = 521 \pm 50$ K for S4 and 560 ± 30 K for S5 and a mid $T_c = 523 \pm 20$ K for S5. These values coincide within experimental error with the $T_c \sim 550$ K determined previously. Cycling above 700 K cause the disappearance of the anomaly in all cases.

Even though there is a kink or a small jump in the resistance, there is no percolation. Considering that superconductivity is granular, percolation should be indeed difficult, if not impossible, to obtain. As discussed previously, superconductivity may be due to ABC/ABA stacking faults²² or "magic angle" between different graphite monocrystals in the HOPG matrix^{11,23}.

We now describe results on the dirtiest and more disordered samples of our lot, expanded carbon foils used as gaskets in refineries or car engines. Grafoil²⁴ and Papyex are similar materials, both being manufactured in a process whereby finely ground particles of mined graphite are intercalated with several substances, then rinsed with water to produce a residue compound. This compound is then subjected to intense heat (900-1200 °C) to initiate exfoliation. The exfoliated graphite is then compressed via rollers into a flexible foil-like material which is able to hold together without the aid of binding agents. Further heating (600 °C) is applied to drive off impurities and any remnant intercalant. It is another intercalation-deintercalation process, similar in principle to the one described in Ref. 16, but more violent.

Zero field cooled (ZFC) and field cooled (FC) measurements on Grafoil and Papyex samples are shown on Fig. 3a and b. Two anomalies at around 70 K and 260 K are present in both samples. Also the diamagnetic signal continues to increase at the highest measured temperature, suggesting another transition at higher temperatures. In both samples, at low temperatures we observe a Curie law type increase, which can be fitted and subtracted from the data. This behavior can be attributed to magnetic impurities, known to exist²⁵ in such industrial products. In both cases the impurities' Curie temperature $T_{0_{imp}} \sim -20 \pm 5$ K, indicating weak antiferromagnetic interactions among impurities. Upon subtraction, the anomaly at low temperatures shows a behavior that has strong similarities with what could be expected from measurements on a superconductor with such a T_c . The transition at higher temperatures is less field dependent.

The evolution with temperature of the ferromagnetic cycles of Grafoil samples obtained by subtraction of the measured diamagnetic linear contribution of bulk graphite is shown for S6 on Fig. 3c. The amplitude of the cycles slowly diminish with temperature. Similar measurements done on Papyex samples yield an analog behavior. We plot on Fig. 3d the temperature dependence of the magnetization saturation at 1 T for two typical Grafoil and Papyex samples. By fitting with expression (1) both dependences we obtain similar values of $T_0 = 562 \pm 50$ K. The values of the saturation magnetization at 0 K are: for S6 $M_0 = 0.026$ emu/gr ($5.2 \times 10^{-5} \mu_B$ per carbon atom) and for S8 $M_0 = 0.002$ emu/gr ($0.4 \times 10^{-5} \mu_B$ per carbon atom).

The temperature dependence of the superconducting-like hysteresis loops obtained by subtraction of the bulk

graphite linear diamagnetism and of the ferromagnetic sigmoidal evolution is shown for the Grafoil sample S8 on Fig. 4a and for Papyex sample S11 on Fig. 4c. We then plot the evolution of $\Delta M(H,T)$, as defined in Fig. 1b, as a function of temperature for the Grafoil and the Papyex samples on Fig. 4c and on Fig. 4d. The overall shape is sharply different from those of HOPG samples. The reason is that, as temperature decreases, we have the transitions at 260K and 70K that appear and start contributing to the thickness of the superconducting-like hysteresis loop that we measured. To separate the effect on the cycles for the different transitions, we first fit with expression (2) only the points above 260K. This fit corresponds to the evolution of the highest temperature transition. Next, we fit the points between the two low temperature transitions, 260K and 70K, and fit with expression (2) plus the fit obtained for the high temperature transition. Finally, we choose the points below 70K and fit with expression (2) plus the fit obtained for the high temperature transition, plus the fit obtained for the intermediate region.

We show the result of the fits on for Grafoil samples S6 and S9 Fig. 4c and for Papyex samples S7 and S10 on Fig. 4d. The green dashed curves correspond to the high temperature transition, $\sim 510 \pm 50$ K for the Grafoil samples and $\sim 623 \pm 50$ K for the Papyex samples, the red dashed curves to the intermediate transition $\sim 275 \text{K} \pm 15$ and $\sim 257 \text{K} \pm 15$, respectively, and the blue dashed lines to the low temperature transition, $\sim 69 \pm 5$ K and $\sim 77 \pm 5$ K, respectively. We show them added (on the experimental points) and separated (at the bottom of the graph).

Discussion

It is interesting to compare the low and intermediate temperature results with those reported for IDI samples in Ref. 16. There, we have also two transitions at temperatures near to the ones observed here, namely 110K and 245K. Considering that the synthesis methods are not fundamentally different we would expect similar transition temperatures. While the low T_c for Grafoil and Papyex is more than 30% smaller than the IDI value, the intermediate T_c is less than 10% higher. It can be that in IDI samples the residual potassium induces a doping different to the one operating in gasket foil samples. On the other hand, perhaps the difference is an effect of the magnetic impurities responsible for the Curie law, absent in IDI samples, lowering only the low T_c value.

We observe that for the HOPG, Grafoil and Papyex samples the high temperature transition is, within the error of the determination, the same at around 550K. It is not astounding that hidden granular superconductivity has been so difficult to detect having such large T_c values compared to room temperature, the highest temperature available in many laboratories that study superconductivity. Furthermore, electrical resistance measurements showed that the observed anomaly disappears by cycling above 700K. As our measurements in the optical oven are very fast (10-20K per minute), it is probable that the crystallites responsible for the anomaly, and superconductivity, are modified at these temperatures. Most probably this is due to changes in doping, as annealing of graphite defects can only be attained nearer to the graphitizing temperature. This fact will certainly be an obstacle for detailed studies around T_c .

We must note that the observed ferromagnetism possibly cannot be totally attributed to ferromagnetic impurities. Firstly, detailed analysis^{19,26} have determined on different types of HOPG samples, including those made by the same company as the ones measured here, that impurities would give a lower measured value. Secondly, and more important, it has been shown that annealing HOPG to temperatures near to the graphitizing temperature, 2400°C, extinguishes²⁷ most of the ferromagnetic signal, implying an origin due to graphite defects. On the other hand, the presence of the magnetic impurities (determined through a Curie law) boosts T_0 to a value that, within measuring error, is the same as the high temperature T_c . This fact is intriguing. It may be just due to some magnetic impurity. If we hypothesize

that it is intrinsic, it might tell us that the maximum value of the Curie temperature of ferromagnetic state issued from the same interaction as the superconductivity that we observe is identical to the maximum superconducting transition temperature $T_{0_{max}}=T_{c_{max}}$. Finally, within the assumption of an intrinsic carbon ferromagnetism, as the number of carriers for graphite is 2.4×10^{-5} electrons and 1.8×10^{-5} holes per carbon atom²⁸, it seems that a sizable number of carriers are spin polarized, although it is clear that the exact number depends on the particular geometry of each sample.

The origin of the observed granular superconductivity is still blurry and speculative. The spread of T_c 's above room temperature can obviously be due to the fact that they are obtained from the extrapolation of a phenomenological fit. From the electrical resistance measurements, though, there seems to be differences due to, perhaps, doping. For the low temperature transitions at around 100K and 250K, seen only in samples obtained from the IDI process that renders bulk twisted graphite¹⁶ and gasket foils made from compressed expanded graphite, the origin may be related to Moiré type defects. While in pure and well crystallized graphite, omnipresent rhombohedral stacking faults have been held as responsible¹¹, even though Moiré defects also exist in well crystallized graphite²⁹. Nonetheless, the physics behind seems to be in both cases that of flat bands. As flat band superconductivity is very strong coupling³⁰, the expression for the superconducting gap instead of being $\Delta \sim \exp[-1/V\rho(0)]$ is $\Delta \sim V\rho(0)$, where V is the superconducting interaction and $\rho(0)$ the density of states at the Fermi level, proportional to the flatness of the band. Thus, while for normal coupling superconductivity an increase of $\rho(0)$ is strongly attenuated by the exponential, in flat band superconductivity it is not, and $T_c \sim \Delta$ is not bounded. Our measurements might be an example. In any case much work is still necessary to confirm, pin down and understand the origin of the superconductivity (and ferromagnetism) in graphite.

Materials and Methods

HOPG samples were obtained from portions of ZYA grade HOPG from Union Carbide derived from a neutron monochromator and of ZYH grade from Neyco. All the HOPG samples were measured with the field parallel to the c graphitic axis. de Haas-van Alphen oscillations of S2 show a clear frequency at 4.8T corresponding to the hole's Fermi surface of $4.7 \times 10^{12} \text{ cm}^{-2}$ of Bernal graphite, a mobility of $2 \times 10^4 \text{ cm}^2/\text{Vs}$ at 5K can be estimated from onset magnetic field of the quantum oscillations. These results confirm the high quality and homogeneity of the samples.

Grafoil samples were cut from a large roll obtained from Union Carbide (presently NeoGraf), while the Papyex-N samples were extracted from a piece furnished by the Carbone Lorraine (presently Mersen) research laboratory. Both materials were thoroughly studied by neutron diffraction previous to studies of ^3He adsorption on graphite²⁵. Contrary to HOPG ZYA and ZYH that have a mosaic spread of 0.4° and 3.5° , respectively, in Grafoil and Papyex the spread is 30° . For the magnetization measurements, stripes were cut that were then folded into a cuboidal shape.

Magnetization measurements were performed in a Quantum Design MPMS3, VSM-Squid Magnetometer, at IN, and two Quantum Design MPMS XL QD at IN and LPS. The sample holder were the thin plastic straws furnished by Quantum design, with no other addenda.

High temperature resistivity measurements were performed in home-made fast optical furnaces at IN, in a four lead DC measurement with four tungsten elastic fingers to ensure the electric contact. Two different apparatus were used, one with four fixed aligned contacts and the other with four fixed contacts in a van der Pauw configuration. For this last one only one configuration opposing current and voltage contacts was measured. This non-linear configuration can be more sensitive to high conductivity defects in a large surface, but the value or even the shape can be approximative

if the alternative opposed current/voltage configuration is not measured at the same time, which was not possible in our apparatus. While the linear configuration can give better results only if they are correctly placed on the defect. Dozens of contact positioning had to be made to locate half a dozen "sweet spots" where transitions were observable.

Acknowledgments

MNR thanks K. Hasselbach, C. Paulsen for discussions and P. Monceau, J.E. Lorenzo-Díaz, M-A. Méasson, O. Buisson, F. Levy-Bertrand for a critical reading of the manuscript. We thank H. Godfrin and M. d'Astuto for providing us with the Grafoil and Papyex samples and the ZYA monochromator, respectively, and A. Hadj-Azzem and J. Balay for technical help. SL acknowledges support from the French National Research Agency through the projects IRONMAN ANR-18-CE30-0018 and MNR from PRESTO ANR-19-CE09-0027.

-
- * Present Address: Department of Physics, School of Engineering, University of Petroleum and Energy Studies (UPES), Dehradun, Uttarakhand 248007, India
- † Corresponding author. E-mail: manolo.nunez-regueiro@neel.cnrs.fr
- ¹ H. K. Onnes, The resistance of pure mercury at helium temperatures. *Commun. Phys. Lab. Univ. Leiden* **12**, 1 (1911).
 - ² J.R. Gavaler, Superconductivity in Nb-Ge films above 22 K, *Appl. Phys. Lett.* **23**, 480 (1973).
 - ³ J. D. Bednorz and K.A. Mueller, Possible high T_c superconductivity in the Ba-La-Cu-O system, *Z. Phys. B-Cond. Matt.* **64** 189-193(1986)
 - ⁴ M. Monteverde, M. Núñez-Regueiro, C. Acha, J. Pshirsov, S. Putilin and E. Antipov, High pressure effects in fluorinated Hg-1223, *Europhys.Lett.*, **72**, 498 (2005)
 - ⁵ A.P. Drozdov, P. P. Kong, V. S. Minkov, S. P. Besedin, M. A. Kuzovnikov¹, S. Mozaffari et al. Superconductivity at 250 K in lanthanum hydride under high pressures. *Nature* **569**, 528–531 (2019).
 - ⁶ E. Snider, N. Dasenbrock-Gammon, R. McBride, M. Debessai, H. Vindana, K. Vencatasamy et al., Room-temperature superconductivity in a carbonaceous sulfur hydride, *Nature* **586** 373 (2020)
 - ⁷ Kuwabara, D. R. Clarke, and D. A. Smith, Anomalous superperiodicity in scanning tunneling microscope images of graphite *Appl. Phys. Lett.* **56**, 2396-2399 (1990).
 - ⁸ Y. Kopelevich, P. Esquinazi, J. H. S. Torres and S. Moehlecke, Ferromagnetic- and Superconducting-like Behavior of Graphite, *J. Low Temp. Phys.* **119**, 691 (2000).
 - ⁹ T. Scheike, W. Böhlmann, P. Esquinazi, J. Barzola-Quiquia, A. Ballestar, and A. Setzer, Can Doping Graphite Trigger Room Temperature Superconductivity? Evidence for Granular High-Temperature Superconductivity in Water-Treated Graphite Powder, *Adv. Materials* **24**, 5826-5831(2112).
 - ¹⁰ R. Ariskina, M. Stiller, C.E. Precker, W. Böhlmann and P.D. Esquinazi, On the localization of persistent currents due to trapped magnetic flux at the stacking faults of graphite at room temperature, *Materials* **15**, 3422(2022)
 - ¹¹ P. Esquinazi, T.T. Heikkilä, Y. V. Lysogorskiy, D.A. Tayurskii, and G.E. Volovik, On the superconductivity of graphite interfaces, *JETP Letters* **100**, 336-339(2014).
 - ¹² G. Chen, A.L. Sharpe, E.J. Fox, Y-H. Zhang, S. Wang, L. Jiang, B. Lyu, H. Li, K. Watanabe, T. Taniguchi, Z. Shi, T. Senthil, D. Goldhaber-Gordon, Y. Zhang, F. Wang, Tunable Correlated Chern Insulator and Ferromagnetism in Trilayer Graphene/Boron Nitride Moiré Superlattice, *Nature* **579**, 56(2020).
 - ¹³ Cao, Y. et al. Unconventional superconductivity in magic-angle graphene superlattices. *Nature* **556**, 43–50 (2018).
 - ¹⁴ G. Trambly de Laissardiére, D. Mayou, and L. Magaud, Localization of Dirac Electrons in Rotated Graphene Bilayers, *Nano Lett.* **10**, 804808 (2010).

- ¹⁵ R. Bistritzer and A.H. MacDonald, Moire bands in twisted double-layer graphene, *PNAS* **108**, 12233-12237 (2011).
- ¹⁶ S. Layek, M. Monteverde, G. Garbarino, M-A. Measson, A. Sulpice, N. Bendjab, P. Rodiere, R. Cazali, A. Hadj-Azzem, V. Nassif, D. Bourgault, F. Gay, D Dufeu, S. Pairis, J-L. Hodeau, and M Núñez-Regueiro, Possible high temperature superconducting transitions in disordered graphite obtained from room temperature deintercalated KC8, ArXiv 2205.09358 (2022)
- ¹⁷ C. Urban, I. Valmianski, U. Pachmayr, A. C. Basaran, D. Johrendt and I.K. Schuller, Coexistence of multiphase superconductivity and ferromagnetism in lithiated iron selenide hydroxide $[(\text{Li}_1 - x\text{Fe}_x)\text{OH}]\text{FeSe}$, *Phys. Rev. B* **97**, 024516 (2018).
- ¹⁸ C.P. Bean, Magnetization of High-Field Superconductors, *Rev. Mod. Phys.* **36** 31(1964)
- ¹⁹ P. Esquinazi, A. Setzer, R. Höhne, C. Semmelhack, Y. Kopelevich, D. Spemann, T. Butz, B. Kohlstrunk, M. Lösche, Ferromagnetism in Oriented Graphite Samples, *Phys. Rev. B* **66**, 024429 (2002).
- ²⁰ G. Zhang, T. Samuely, Z. Xu, J.K. Jochum, A. Volodin, S. Zhou, P. W. May, O. Onufrienko, J. Kacmarcik, J. A. Steele, J. Li, J. Vanacken, J. Vacik, P. Szabo, H. Yuan, M. B. J. Roeflaers, D. Cerbu, P. Samuely, J. Hofkens, and V. V. Moshchalkov, Superconducting Ferromagnetic Nanodiamond, *ACS Nano*, **11**, 5358(2017).
- ²¹ C. Paulsen, D. J. Hykel, K. Hasselbach, and D. Aoki, Observation of the Meissner-Ochsenfeld Effect and the Absence of the Meissner State in UCoGe, *Phys. Rev. Lett.* **109**, 237001(2012).
- ²² A. Hentrich and P. D. Esquinazi, Effects of the Stacking Faults on the Electrical Resistance of Highly Ordered Graphite Bulk Samples, *C-J. of Carbon Res.* **6**, 49 (2020).
- ²³ T. Cea, N. R. Walet and F. Guinea, Twists and the Electronic Structure of Graphitic Materials, *Nanolett.* **19**, 8683-8689(2019).
- ²⁴ J. H. Shane, R. J. Russell, and R. A. Bochman. "Flexible Graphite Material of Expanded Particles Compressed Together". U.S. pat. 3404061A. Union Carbide Corp. Oct. 1, 1968.
- ²⁵ H. Godfrin and H-J. Lauter, Experimental properties of the ^3He adsorbed on graphite, in *Progress in Low Temperature Physics*, vol. XIV, Edited by W.P. Halperin, Elsevier Science (1995)
- ²⁶ D. Spemann, P. Esquinazi, A. Setzer, and W. Böhlmann, Trace element content and magnetic properties of commercial HOPG samples studied by ion beam microscopy and SQUID magnetometry, *AIP Advances* **4**, 107142 (2014).
- ²⁷ X. Miao, S. Tongay, A. F. Hebard, Extinction of ferromagnetism in highly ordered pyrolytic graphite by annealing, *Carbon* **50** 1614-1618(2012)
- ²⁸ J.W. McClure, Band structure of graphite and de Haas-van Alphen effect, *Phys. Rev.* **108**, 612(1957) .
- ²⁹ F. S. Boi, G. Shuai, J. Wen and S. Wang, Unusual Moiré superlattices in exfoliated μm -thin HOPG lamellae: An angular-diffraction study, *Diamond and Related Materials* **108** 107920(2020)
- ³⁰ G.E. Volovik, Graphite, Graphene, and the Flat Band Superconductivity. *JETP Lett.*, **107**, 516–517(2018).

TABLE I. Sample description.

Sample number	Type	Company	Measurement	T_c 's(K)
S1	HOPG ZYA	Union Carbide	Magnetization	531K
S2	HOPG ZYA	Union Carbide	Magnetization	573K
S3	HOPG ZYH	Neyco	Magnetization	554K
S4	HOPG ZYA	Union Carbide	Resistance	521K
S5	HOPG ZYA	Union Carbide	Resistance	560K
S6	FGG Grafoil	Union Carbide	Magnetization	69K; 275K; 510K
S7	FGG Papyex	Carbone Lorraine	Magnetization	67K; 266K; 534K
S8	FGG Papyex	Carbone Lorraine	Magnetization	77K; 257K; 623K
S9	FGG Grafoil	Union Carbide	Magnetization	69K; 275K; 510K
S10	FGG Papyex	Carbone Lorraine	Magnetization	77K; 257K; 623K

Figures

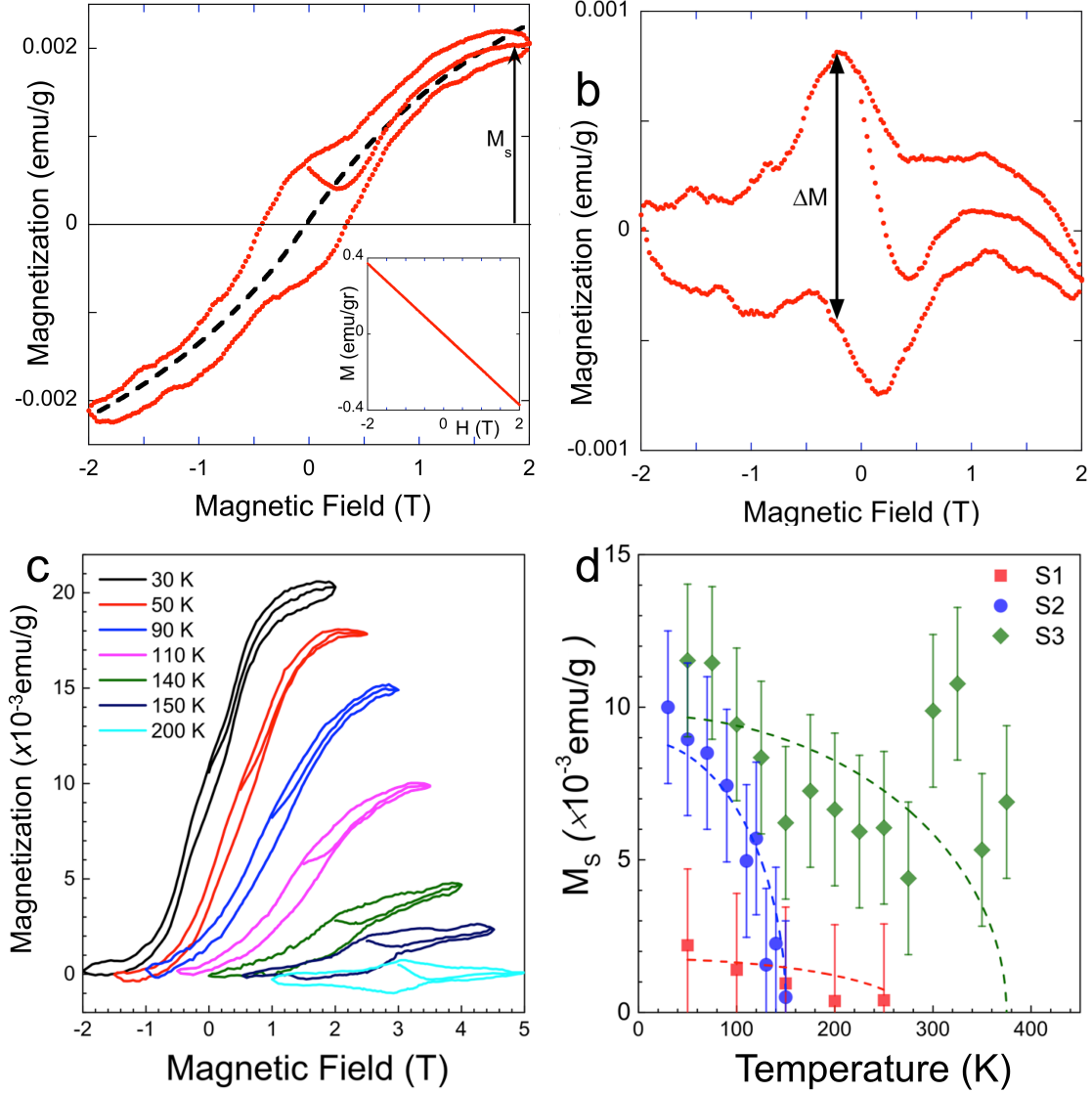


FIG. 1. (a) Ferromagnetic hysteresis cycle after subtraction of the graphite diamagnetic contribution of S1 at 50K. An unexpected bulge due to superconductivity is present around zero ($H//c$). Dashed line: Ferromagnetic type sigmoidal fit. inset: raw data showing the strong linear diamagnetic magnetization that must be subtracted to obtain the "hidden" ferromagnetic signal. (b) Superconducting-like hysteresis loop after subtraction of the ferromagnetic sigmoidal fit typical of a superconducting state. (c) Ferromagnetic cycles obtained after subtraction of the diamagnetic graphite contribution at different temperatures for S2. For clarity reasons we have defined the zero of magnetization at the beginning of the cycle and shifted each curve by 0.5T. At 150K, ferromagnetism has almost disappeared, and the cycle has become completely diamagnetic at 200K. (d) Saturation magnetizations as a function of temperature for samples S1 (red squares), S2 (blue circles) and S3 (green diamonds). Dashed curves: fits with the phenomenological function (1).

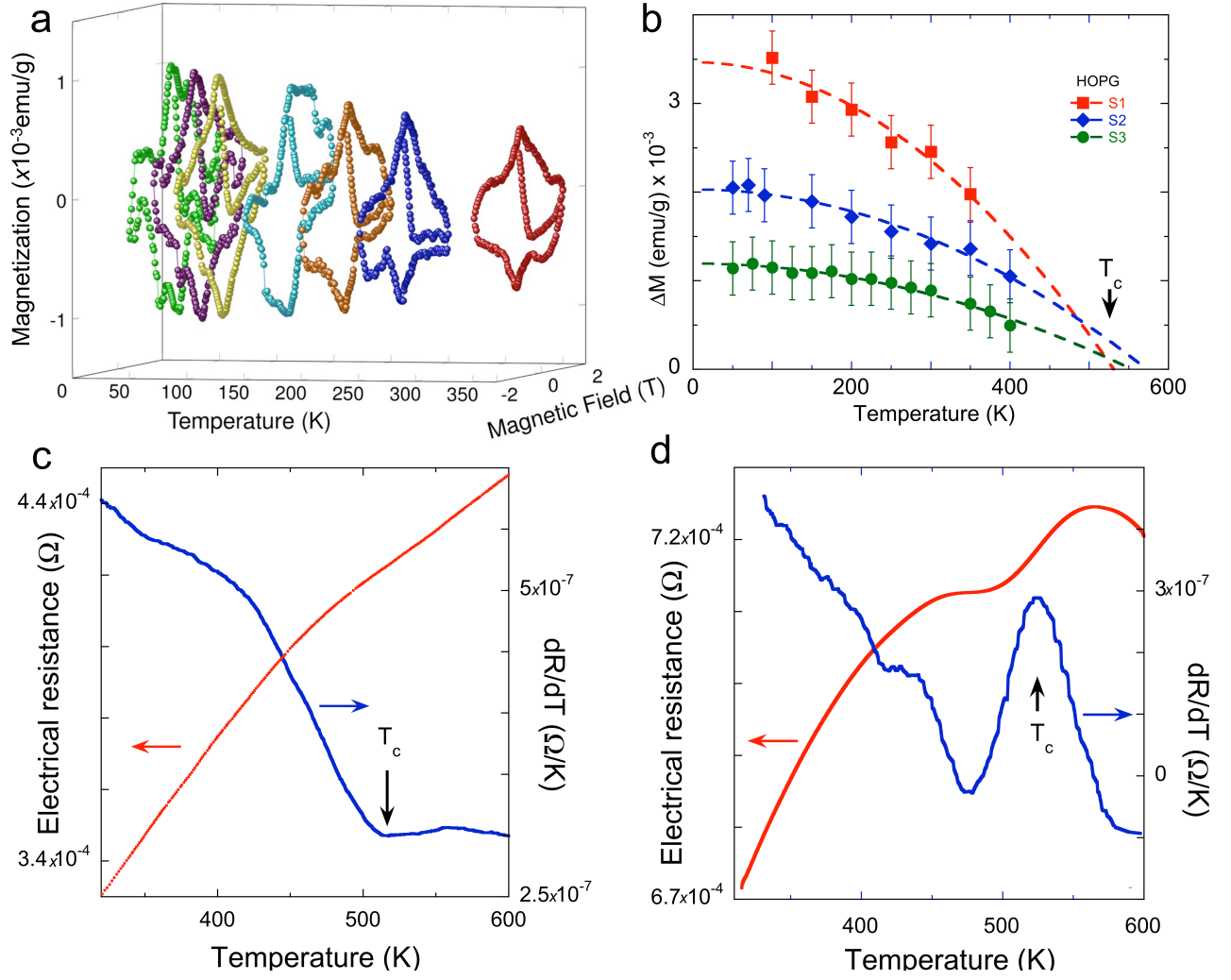


FIG. 2. (a) 3D plot of the superconducting-like hysteresis loops obtained by subtraction of the diamagnetic graphite contribution and the ferromagnetic sigmoidal fit for S2. We observe that the cycles decrease in amplitude with increasing temperature. (b) Temperature dependences of the amplitude ΔM of the cycles at $H = -0.1 \text{ T}$, as defined in Fig. 1, for S1 (red squares), S2 (Blue diamonds) and S3 (green circles). As $\Delta M(H, T) \sim J_c(H, T)$ we fit the dependences with the known expression (2) for the temperature dependence of $J_c(H, T)$ (dashed curves), that allows determining an average $T_c \sim 550 \pm 50 \text{ K}$ for these HOPG samples. (c) (red line) Temperature dependence of the electrical resistance with four aligned contacts in sample S4; (blue line) derivative of the electrical resistance as a function of temperature showing a transition with an onset $T_c \sim 521 \pm 50 \text{ K}$. (d) (red line) Temperature dependence of the electrical resistance in van der Pauw contact configuration for S5 (see discussion on resistance measurements in Materials and Methods); (blue line) derivative of the electrical resistance as a function of temperature showing a transition at mid transition $T_c \sim 523 \pm 20 \text{ K}$, and an onset $T_c \sim 560 \pm 30 \text{ K}$.

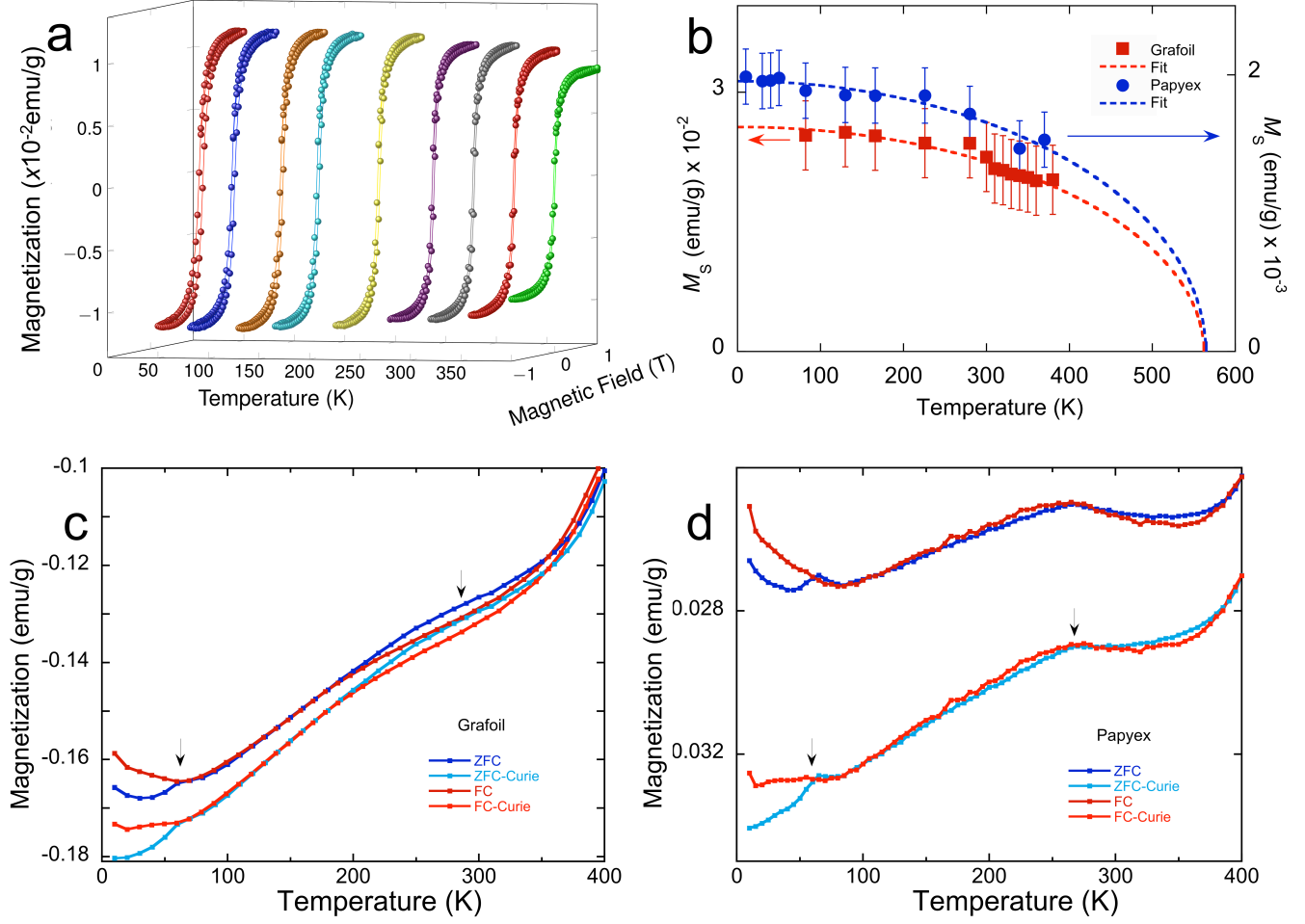


FIG. 3. (a) 3D plot of the ferromagnetic cycles of the Grafoil sample S6, obtained by subtracting only the linear diamagnetic graphite contribution from the raw data. We observe that the cycles decrease in amplitude with increasing temperature. (b) Saturation magnetizations as a function of temperature for samples Grafoil S6 (red squares) and Papyex S7 (blue circles). Dashed curves: fits with the phenomenological function (1). (c) Zero field cooled and field cooled temperature magnetization measurements at 1T for Grafoil sample S6. We observe two transitions at ~ 270 K and ~ 70 K. Upper curves: For the raw data we observe at low temperatures a Curie paramagnetic law that can be fitted and subtracted. Lower curves: upon subtraction of the Curie law we obtain what seems to be the signature of a superconducting transition at ~ 70 K. (d) Similar as (c) but at 3T for Papyex sample S8.

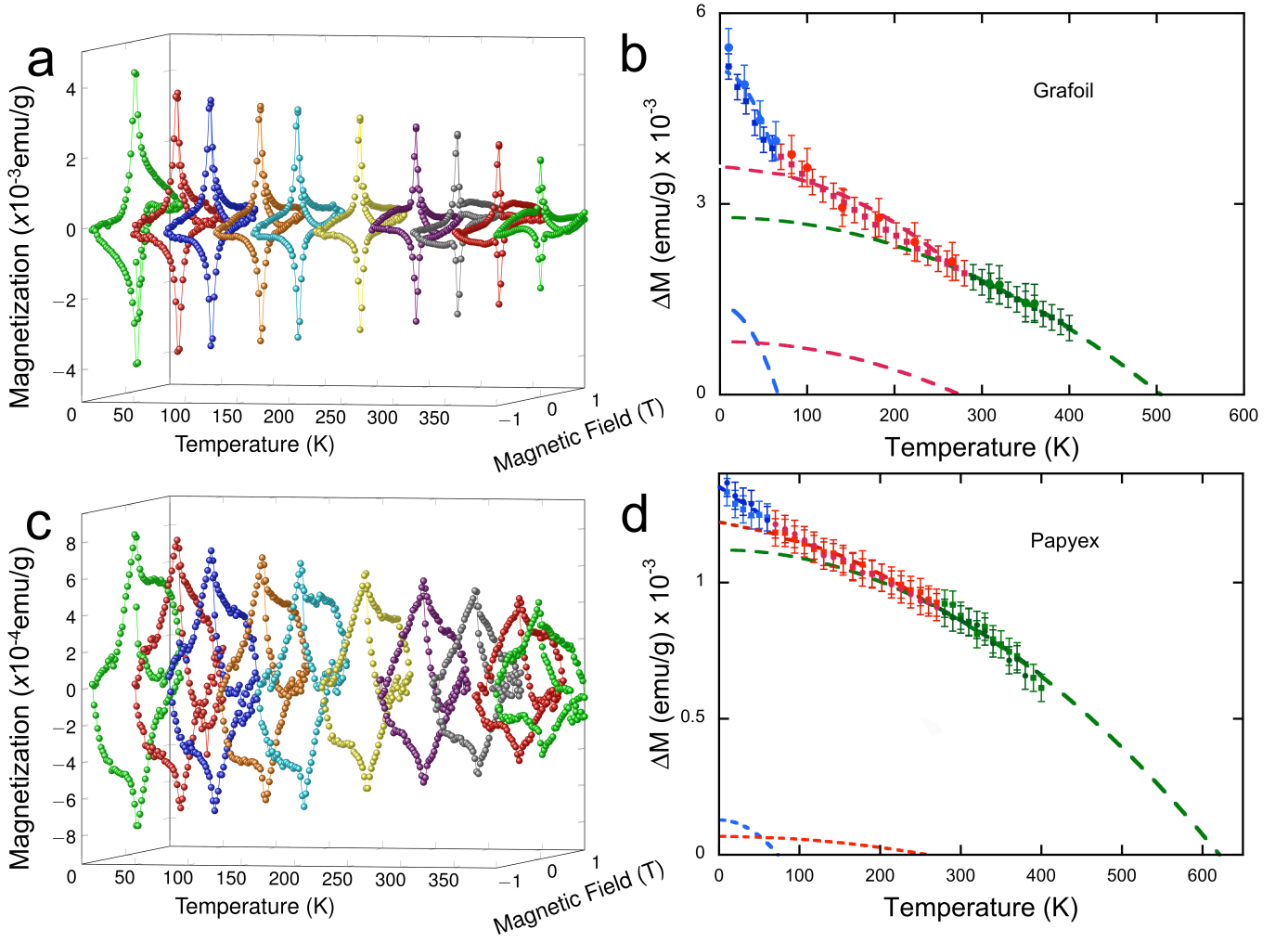


FIG. 4. (b) Evolution of the superconducting-like hysteresis loops extracted by subtraction of the linear graphite contribution and a sigmoidal contribution (as in Fig. 1) for Grafoil sample S9. (b) Temperature dependences of the amplitude ΔM of the cycles at $H=-0.08\text{T}$, as defined in Fig. 1, for Grafoil samples S6 and S9. As $\Delta M(H,T) \sim J_c(H,T)$ we fit the dependences with the known expression (2) for the temperature dependence of $J_c(H,T)$ (dashed curves), that allows determining three average $T_c \sim 510 \pm 50\text{K}$, $T_c \sim 275\text{K} \pm 15$ and $T_c \sim 69 \pm 5\text{K}$ (details in text). (c) Evolution of the superconducting-like hysteresis loops extracted by subtraction of the linear graphite contribution and a sigmoidal contribution (as in Fig. 1) for Papyex sample S8. (d) Temperature dependences of the amplitude ΔM of the cycles at $H=-0.08\text{T}$, as defined in Fig. 1, for Papyex samples S8 and S10. As $\Delta M(H,T) \sim J_c(H,T)$ we fit the dependences with the known expression (2) for the temperature dependence of $J_c(H,T)$ (dashed curves), that allows determining three average $T_c \sim 623 \pm 50\text{K}$, $T_c \sim 257\text{K} \pm 15$ and $T_c \sim 77 \pm 5\text{K}$ (details in text).